Optical Fiber Bragg Grating Strain Sensor for Bone Stress Analysis in Bovine During Masticatory Movements

Alessandra Kalinowski, Leandro Zen Karam, Vinicius Pegorini, André Biffe Di Renzo, Christiano Santos Rocha Pitta, Rafael Cardoso, Tangriani Simioni Assmann, Hypolito José Kalinowski, and Jean Carlos Cardozo da Silva

***Abstract*— This paper describes an optical-fiber sensor development and implementation, based on Bragg gratings, to measure the mechanical deformation at the bone surface of a bovine mandible, caused by chewing different types of food and rumination. A suitable encapsulation was developed using a titanium mesh as a transducer and sensor calibration and characterization tests were performed. The proposed sensor was deployed in a living animal transmitting the detected bone deformation to the data collecting instrument. The acquired signal was applied to a pattern-classification algorithm based on decision trees for identifying the chewing process of different foods. The results demonstrate that the sensor is effective and sensitive, capable of capturing the force generated during the masticatory process.**

***Index Terms*— Biomechanics, biosensor, Bragg gratings, in vivo monitoring, optical-fiber sensors.**

I. Introduction

In 1892, Julius Wolff and co-authors realized that mechanical loads could affect the bone architecture in living beings (Wolff's law) [1]. Currently, there is a consensus in the literature over the fact that mechanical stress is a major contributor to cell differentiation process, which defines the matrix between osteoblasts and osteoclasts [1]–[3]. Thus, knowing this cellular process, health professionals can assess and plan bone fracture repair process, as well as bone adaptation to materials implanted into the organism.

Bone deformation measurement also attracts attention from livestock area professionals. The acquisition and analysis of chewing movements in ruminants through bone deformation measurements allow the characterization of chewing patterns, which are important for further advances in instruments and techniques for the evaluation of animals' feeding behavior. The monitoring of food consumption of these animals helps in determining pastures productivity and provides information about the health and well-being of the animal [4]. Thus, it is relevant to the used approaches to identify the different aspects involved in the ruminant grazing process.

Different techniques have been employed to assess the ingestion behavior of animals in grazing environments. The acoustic method is the main ingestive monitoring technique used [4], [5]. This technique uses audio sensors to obtain data on mandibular movements of animals during the grazing period. Another widely used alternative is direct observation, wherein observers collect data from chewing and piece, during feeding process [6]. There is also a technique based on fecal analysis for the evaluation of the aliment intake [7]. Although these techniques are not invasive, most of the data collection and their transcript into appropriate analysis software is done manually, and thus are prone to human errors that can induce inaccurate results.

Another way to observe the ruminant's ingestive behavior is through esophageal fistula technique [8]. This technique consists of performing a surgical procedure in which the animal is sedated and an incision in the esophagus is made for the installation of a cannula, responsible for food diversion to a collection bag. Subsequently, feeding data is analyzed using the retrieved material from the collection bag [8]. This technique is rather invasive and can present several issues to the animal's well-being.

To monitoring biomechanical parameters, conventional sensors based on piezoresistive (strain gauges) are used. They represent a highly tested technology, offering good sensitivity, precise measurements and competitive price. However, their miniaturization, for minimally invasive procedures, presents some drawbacks, which, combined with low biocompatibility of metal components and high sensitivity to electromagnetic interference may compromise some *in vivo* applications and their use in clinical practice [9]. In terms of patient comfort, FBG sensors can use a thinner cable to connect the sensor to the monitoring electronics, as compared to conventional 4-wire strain gauges.

Manuscript received January 13, 2017; revised February 6, 2017; accepted February 7, 2017. Date of publication February 9, 2017; date of current version March 22, 2017. The associate editor coordinating the review of this paper and approving it for publication was Dr. Carlos R. Zamarreno. This work was supported in part by the Coordenação de Aperfeiçoamento de Pessoal de Nível Superior, in part by the Conselho Nacional de Desenvolvimento Científico e Tecnológico, in part by the Financiadora de Estudos e Projetos, and in part by the Fundação Araucária and Federal University of Technology-Paraná.

L. Z. Karam is with the Pontifical Catholic University of Paraná, Curitiba 80215-901, Brazil (e-mail: leandro.karam@pucpr.br).

C. S. R. Pitta is with the Federal Institute-Paraná, Palmas-PR 85555-000, Brazil (e-mail: christiano.pitta@ifpr.edu.br).

H. J. Kalinowski is with Departamento de Engenharia de Telecomunicações, Universidade Federal Fluminense, Niterói-RJ 24210-240, Brazil (e-mail: hjkalinowski@id.uff.br).

A. Kalinowski, V. Pegorini, A. B. Di Renzo, R. Cardoso, T. S. Assmann and J. C. C. da Silva are with the Federal University of Technology-Parana, Curitiba-PR 80230-901, Brazil (e-mail: ale.k11@hotmail.com; vinicius@utfpr.edu.br; renzo@alunos.utfpr.edu.br; rcardoso@utfpr.edu.br; tangriani@utfpr.edu.br; jeanccs@utfpr.edu.br).

Digital Object Identifier 10.1109/JSEN.2017.2667618

The development of optical-fiber sensors using fiber Bragg gratings (FBG) to monitor *in vivo* biomechanical parameters attracted attention since the turn of the century [10], [11] because of FBG intrinsic characteristics.

FBG sensors are sensitive to temperature and strain changes [12]. They are also chemically stable and have a reduced size, in the order of millimeters in length and micrometers in diameter, facilitating the implementation into small and irregular locations [9], [13], [14]. In addition, it highlights its biocompatibility and immunity to electromagnetic interference [15], [16]. The FBG characteristics have also found a niche in bone strain measurements and similar applications. Particularly, several authors reported using FBG sensors for bone strain measurements and applications, including *ex vivo* and *in vivo* measurements [15], [17]–[20].

The FBG sensor also permitted *in vitro* assays [19]. Chewing movements were replicated in a goat cadaveric skull, simulating the chewing of two plasticines with different textures. A FBG sensor was used to detect bone deformation, attached to the mandible ramus, close to the articulation, and a classifier was used to recognize chewing signal patterns from plasticines. For two masticatory patterns, this study pointed 100% accuracy in chewed materials recognition, showing FBG sensor's efficiency, in addition to a good signal/noise ratio.

Later, a similar sensor underwent *ex vivo* tests [21]. Chewing movements were reproduced in a bovine head recently discarded by the food industry. The signal was obtained from the chewing of two plasticines with different textures, and also from masticatory movements without any material between dental arches. In this test, the operator performed masticatory movements through mandible external manipulation. The pattern signal acquired by chewing was subjected to a pattern classifier, which provided, for three masticatory patterns, 5% error rate, once more showing FBG sensor's efficiency.

Recently the use of a FBG sensor to monitor the ingestion process of ruminants and to analyze the feed process was reported [20].

This work presents the development of an improved biosensor based on FBG for monitoring bone deformation and relate it with chewing patterns of living animals. The sensor uses a pre-assembly with a proper orthopedic mesh, and it detects bone deformation with a minimally invasive instrument, capable of providing long-term data to an automated pattern-classification system [20]. This application also allows the study to start on bone tissue behavior through the developed sensor.

The paper is organized as follows: Section II presents the procedure descriptions for the biosensor development and its application; in Section III, the results of these experiments are disclosed, along with their discussion; and Section IV reports the conclusions.

II. Materials and Methods

Monitoring mandibular motion involves a lot of care related to the sensor's positioning and its mounting, since the mandible has a non-uniform bone surface and, as published studies in the field reveal, the force distribution is quite irregular [22], [23]. Different types of adhesives were tested to attach the sensor directly to the bone [21]. However, wet and irregular tissue conditions did not allow an efficient adhesion, thereby demonstrating the need for a biosensor development with suitable encapsulation. The encapsulation must be composed of a biocompatible transducer, which makes the sensor less fragile and it must provide a mechanical fixing system so that collage problems are eliminated. Additionally, the encapsulation must be able to transfer deformations to the sensor's location satisfactorily.

A. Biosensor Development

In this paper FBG are used, it is a periodic structure that induces a forbidden band around Bragg's wavelength, preventing propagation of light with frequencies within that band, performing as a selective reflector. Functionally, Bragg gratings have similar behavior to electronic band-notch filter. An important FBG's feature is the fact that external perturbations, such as stress, and temperature variations alter the central reflected wavelength. This spectral encoding reduces problem derived from noise intensity that affect other types of sensors, and facilitates calibration. When an FBG is illuminated by an optical broadband source, only the forbidden band, centered around the Bragg wavelength, is reflected, whereas wavelengths outside that band are transmitted. Bragg's condition is given by [18]:

$$\lambda_B = 2n_{eff}\Lambda, \tag{1}$$

where λ_B is the Bragg's wavelength, Λ is the periodic modulation of the refractive index, and n_{eff} is the effective refractive index of the propagating mode in the fiber core. The effective refractive index and the periodic spacing between FGB planes are affected by changes in temperature or deformation, which will shift the FBG reflected spectrum as described by [12]:

$$\Delta\lambda = \Delta\lambda_{B,l} + \Delta\lambda_{B,t} \tag{2}$$

$$\Delta\lambda = 2\left(\Lambda\frac{\partial n}{\partial l} + n\frac{\partial\Lambda}{\partial l}\right)\Delta l + 2\left(\Lambda\frac{\partial n}{\partial T} + n\frac{\partial\Lambda}{\partial T}\right)\Delta T \tag{3}$$

$$\Delta\lambda = S_l\Delta l + S_T\Delta T, \tag{4}$$

where n is the refractive index, Δl is the deformation and ΔT is the temperature variation, $\Delta\lambda_{B,l}$ is the wavelength change due to the strain, and $\Delta\lambda_{B,t}$ is the shift due to temperature changes. S_l and S_T represent the FBG sensitivities to strain and temperature.

The used FBG were written in Draktel® single-mode optical fiber intended for telecommunications use. The direct illumination method under a phase mask was used to produce the gratings. In the recording process, an excimer laser (KrF) was used with a central wavelength of 248 nm, 5 ns pulse, adjusted to 7 mJ pulse energy and 250 Hz repetition rate. An iris with approximately 3 mm opening defines the Bragg grating length. The resultants FBG have reflectivity greater than 70% and 0.3 nm bandwidth, with Bragg wavelengths centered at 1540 nm.

To reduce the pristine FBG fragility, it was decided to use a titanium surgical mesh as a transducer. The titanium mesh

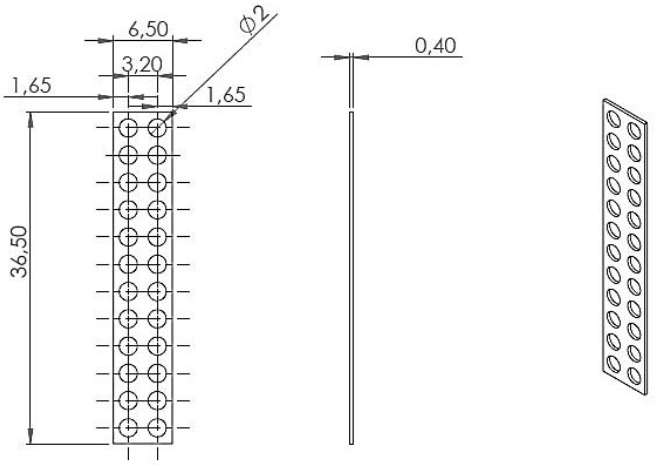

Fig. 1. Titanium mesh drawing with the dimensions used (in mm).

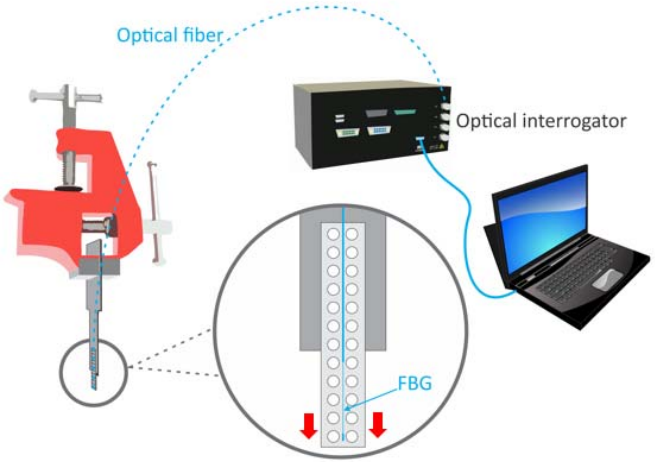

Fig. 2. Schematic layout of the used equipment to sensor's traction experimental test.

was chosen because it is widely used in surgical procedures, so it is a material with well-studied properties [24].

Despite the apparent hardness of the material, its geometry with orifices provides some deformation, as well as facilitating screw attachment to the bone. This material tolerates temperatures from autoclave heating. Its bioinertness and exceptional corrosion resistance in the physiological environment, imparts excellent biocompability [25].

To select the mesh's best region for FBG's collage, it was necessary to know the force components that act on it. To this end, the titanium mesh passed for a traction simulation made with SolidWorks® software, so that the stress regions were known.

Fig. 1 depicts the mesh design with its dimensions, as input in the simulation software. The mesh is supplied in a standard size, and for the desired purpose, it was necessary to cut it using recommended scissors for cutting metallic materials. The mesh size should also be in accordance with the animal's mandible area. The length must be sufficient to accommodate the sensor (3 mm length) and space is also necessary to accommodate the optical cable that protects the fiber during the surgery and the essay. The mesh width must be sufficient to attach it with screws to the animal's bone appropriately.

In the traction simulation, the titanium mesh was fixed by one and two of its orifices in the central region, while the load was applied to the other apertures in its end. The used force was chosen accordingly to those estimated for the experimental calibration test. A 0.588 N force was considered as the load for the simulation.

The sensor was calibrated in the experimental setup described by the layout in Fig. 2. The FBG was glued with cyanoacrylate on titanium mesh, the mesh was fixed by one of its ends with screws to a metal plate, and at the other end were applied progressive loadings directly at the selected holes of the titanium mesh. The load procedures was repeated 10 times with a force range from 0 to 0.588 N, using a step of 0.098 N.

The optical-fiber sensor was connected to a Micron Optics® sm130 interrogator, with 1 pm resolution, and it was connected to a computer, which used Catman®Easy software for acquisition and data processing.

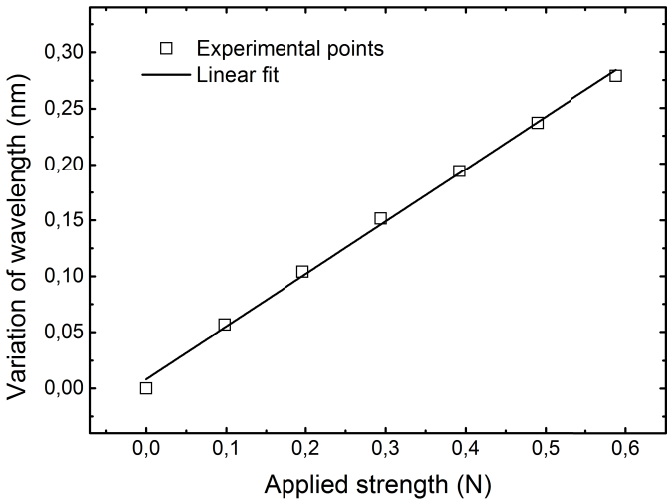

Fig. 3. Sensor's response in wavelength (nm) to applied load (N), with the associated linear fit.

Experimental tests were performed in the laboratory with a controlled temperature of 24 °C (±1 °C). This sensor is designed to be applied in live animals. In a homeostasis state, the temperature change is small and slow, so it will not be a limiting factor for the intended application.

It is noteworthy that the signal acquired from the FBG is analyzed at wavelength, and that changes in signal amplitude, caused by curvatures in the optical cable for example, do not affect the signal reading.

After data acquisition in the calibration procedure, a linear relationship was obtained between the wavelength shift and the applied force to the sensor, and a statistical analysis was performed to verify the uncertainties that the sensor can present in its results. As the test site temperature was controlled, temperature errors were not considered in the uncertainty. The uncertainty sources considered in this work are: type A (sample dispersion) and type B (optical interrogator resolution and linear regression) [26].

The metrological characteristics of the sensor obtained from experimental setup presents a fairly linear response to the load, as can be seen in Fig. 3. The correlation coefficient is

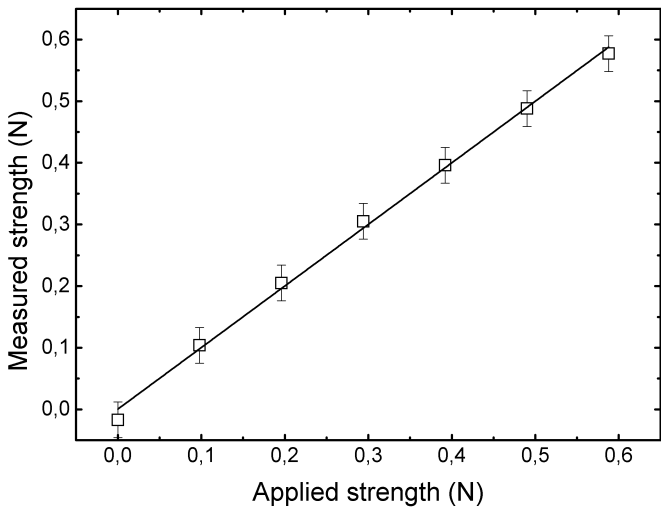

Fig. 4. Relationship between the applied force ratio (N) and the measured force (N) by the sensor, with uncertainty bar and linear fit.

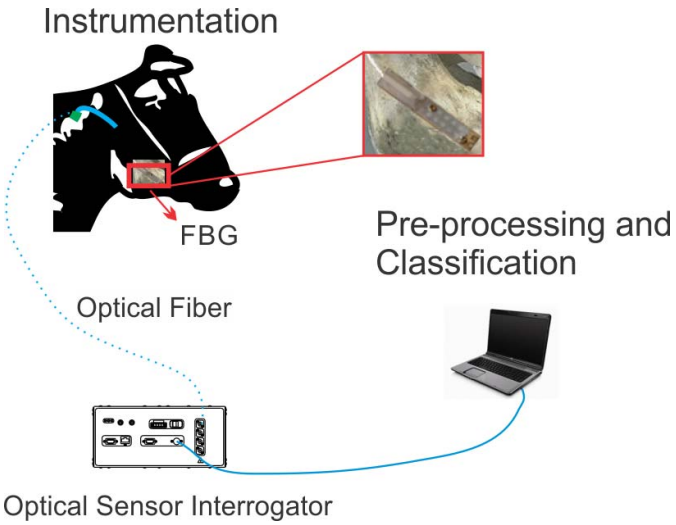

Fig. 5. Bovine instrumentation diagram and data acquisition systems arrangement.

calculated as 0.9987, and the obtained slope is 468 pm/N, according to the linear fit applied to the experimental points.

For each uncertainty, an expanded uncertainty calculation was carried out; we used a t-student table distribution with 95.45% coverage probability [26]. Finally, the combined standard uncertainty was obtained. This calculation uses all the expanded uncertainties evaluated earlier.

The uncertainty combined obtained value from statistical analysis is 0.027 N. The graph showing the relationship between the applied force and the measured force can be observed in Fig. 4, along with the uncertainty bar. The obtained slope is 0.9989, according to the linear fit applied, this data demonstrate the sensor accuracy.

Calibration results indicate good sensitivity. FBG sensors are commonly compared with strain gauges in relation to this parameter, with similar results [27]. The advantage of using FBG is the possibility of *in vivo* applications. FBG's are smaller, easier to implement, minimally invasive, with lower risk of infection, highly accurate and multiplexable, are some of the advantages of the FBG compared to SG [9], in addition, optical fibers sensors can use a thinner cable to connect the sensor to the monitoring electronics.

B. Surgical Procedure

The animal used in the research was a 4-month-old bovine, male, and with a mass of 160 kg. The tests are performed with the approval of the Ethics Committee on Animal Use of the Federal University of Technology – Paraná (protocol CEUA 2013-009).

Before fixation, the biosensor was duly sterilized by autoclave, placed in a surgical grade, and subjected to a 30-min cycle at temperatures of 132-135 °C. This implies minimizing the contamination risks without affecting the sensor's proper performance [28].

Initially, the animal remained without solid or water intake for an interval of 24 h. In the initial stage of the surgical procedure, 2% xylazine hydrochloride anesthetic was used at a dose of 0.3 mg/kg until pharmacological effects are observed. An incision was performed with a 22 cm sterilized scalpel. Other surgical procedures were performed with the aid of straight scissors stainless tip blunt/blunt, rat-tooth forceps size 16 cm, Martin tweezers, and a bone scraper. During the surgical procedure, tissues were folded laterally so that the mandibular bone was exposed and it was possible to fix the biosensor with self-drilling screws.

After fixing the sensor, a simple suture, internal and external knots, is made using a needle-type door 16 cm (Mayo Hegar), a curved stainless steel needle, with a triangular tip and size 6 cm between the ends and nylon thread size 2-0. Once the surgical procedure is closed, to the animal was applied oxytetracycline (dihydrate) 20% at a dose of 1 ml/10 kg body mass via intramuscular route. The same dosage is applied twice with an interval of 3 days, totaling three applications. There was a 7-day interval between the surgical process and the feeding process for data acquisition.

The sensors fixing location was determined from previous work that assessed the force distribution in a human mandible model [22], [23], and also in animal mandible models [19], [21]. The sensors fixing location of the animal's jaw was chosen because is related to a bone region where the forces from the masticatory muscles act sharply, so this region becomes suitable for fixing the sensor because it generates more information about bone deformation when compared to other regions of the jaw.

Fig. 5 demonstrates the bovine instrumentation diagram, indicating sensor fixing location and data acquisition system.

C. Acquisition and Signal Processing

For the acquisition of optical signal and data collection, a Micron Optics® sm130 interrogator, with 1 pm resolution, was used with Catman®Easy software. The sampling rate used in the tests was 1,000 samples per second. The analysis was done 7 days after the surgery, the animal was already feeding normally.

Fig. 6. Calf feeding, with the implanted sensor, seven days after surgery.

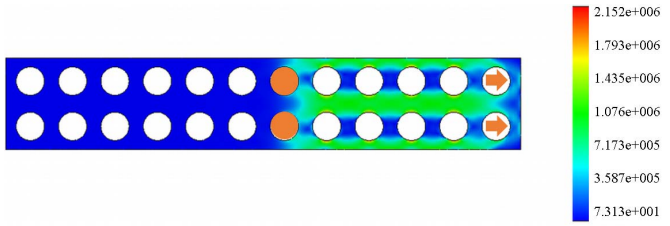

Fig. 7. Stress regions acting on the titanium mesh produced by SolidWorks® software with two attachment points and two force application points. Scale in N/m^2.

The first ingested food was cattle ration, for 13 min. Then, it was served hay (a dried grass and vegetable mixture) ingested for an approximate time of 10 min. The third offered food was ryegrass (a grass type) for an approximate intake time of 5 min. After the chewing process of the three types of foods, the animal rested for about 45 min until it started the rumination lasting approximately 15 min. The photograph in Fig. 6 shows the animal eating with the implanted sensor. In blue, the optical cable can be seen.

The obtained signals were applied to a pattern classifier based on decision trees, which was developed for this specific application, detailed in [20].

III. Results and Discussion

From the numerical model generated in the SolidWorks® software, it was possible to determine an appropriate area for bonding the FBG.

Fig. 7, 8 and 9 were generated as a result of the simulation with 10 N of load. It can be seen that the mesh fixing is performed at its middle section, considering that half of it will be used for the optical cable fixing. The attachment points are indicated by the orange circles and arrows indicate the points where the force was applied.

In Fig. 7, 8 and 9, lower strain regions are observed in the dark blue region between the orifices in the horizontal plane, while higher strain regions are identified in clear blue and green regions. In the apertures' central region, where

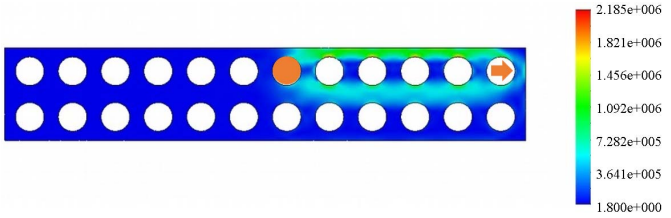

Fig. 8. Stress regions acting on the titanium mesh produced by SolidWorks® software with one attachment point and one force application point aligned. Scale in N/m^2.

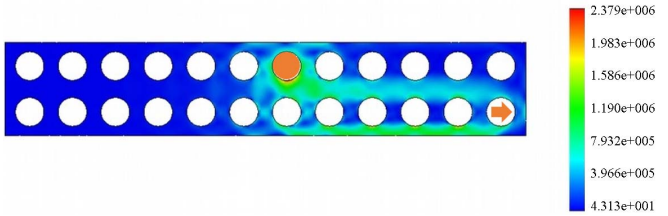

Fig. 9. Stress regions acting on the titanium mesh produced by SolidWorks® software with one attachment point and one force application point misaligned. Scale in N/m^2.

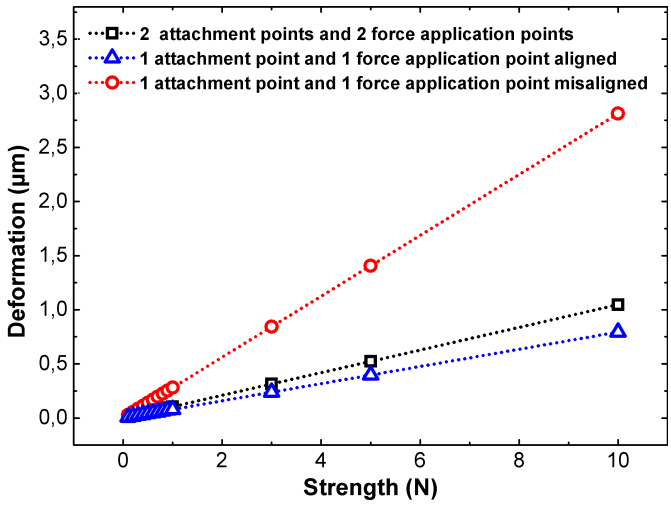

Fig. 10. Relation between deformation in the central region of the titanium mesh and applied force produced by SolidWorks®software.

the sensor is attached, the force components are uniform, proving to be a suitable area for bonding the sensor. This simulation was performed to analyze strain, measurements were given in N/m^2. A new simulation was performed in SolidWorks® software, to analyze deformation in the central region of the mesh, varying the force from 0 to 10. The measurements are now analyzed in μm.

Fig. 10 shows that the mesh with setting configuration of Fig. 9 has a higher sensitivity compared to the other settings, this attachment to the animal reduces the possibility of bone crack and reduces stress during surgery, enabling a faster recovery. So, the simulations showed that Although the configuration of Fig. 7 shows greater tension in the central region of the orifices, this configuration is less sensitive compared to the test with only a force application point misaligned with the fixation point.

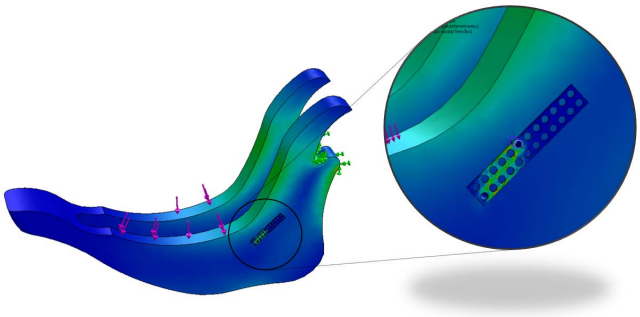

Fig. 11. Mesh attached to bovine mandible designed in the software.

Fig. 12. Encapsulated sensor attached to the bone with screws placed like indicated at the numerical model. Here, part of the optical cable wrapped by silicone tube and the sensor covered by the tape microporous can be seen.

Therefore, this attachment configuration (Fig. 9) was chosen to undergo a new simulation in software, in which the mesh was attached to a designed bovine mandible. The joint region of the mandible was fixed and a force was applied in the region of the teeth, to demonstrate that the force distribution in the titanium mesh remains similar as can be seen in Fig. 11, even if the force is applied in another direction.

Continuing the sensor's mounting, the FBG was glued on the central region of the titanium mesh using cyanoacrylate glue.

Cyanoacrylate-based glues are commonly used in medicine [29], [30] and present a good fixation. The FBG position is indicated in the highlighted circle of Fig. 2.

Once the FBG was bonded to the mesh, it was necessary to cover the optical fiber pigtail with a biocompatible material. The material should protect the fiber against shearing forces to which the fiber would be susceptible after implantation. It was chosen to use a biocompatible silicone cannula, commonly used for implantable catheter manufacture, supplied by IBEG® Company. Over the sensor, fiber pigtail and optical cable length a medical use microporous adhesive tape was placed, in order to increase the sensor strenght. A photograph of the sensor is given in Fig. 12.

The screws used for attachment of the sensor to the animal's bone are of the self-drilling model. For practical ease, reduction surgical stress and other reasons cited above, the configuration for fixing the mesh to the bone was chosen with two asymmetric fixing points, as can be seen in Fig. 12.

The data acquired for each chewed food are described in [20], Fig. 13 depicts detected force *versus* time during the

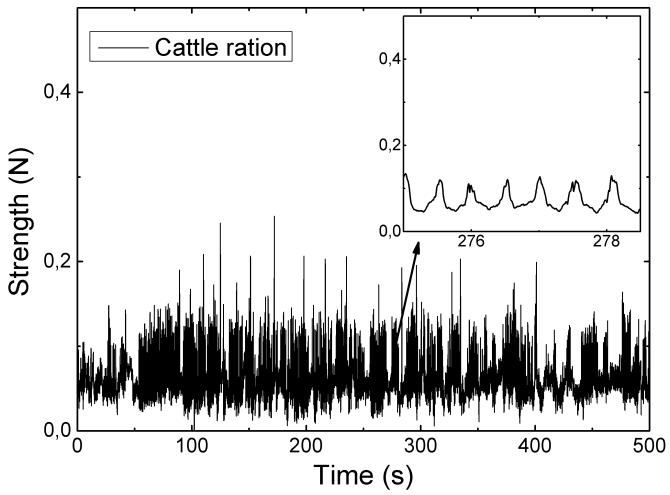

Fig. 13. Graph showing the detected force (N) for chewed cattle ration, in relation to time (s).

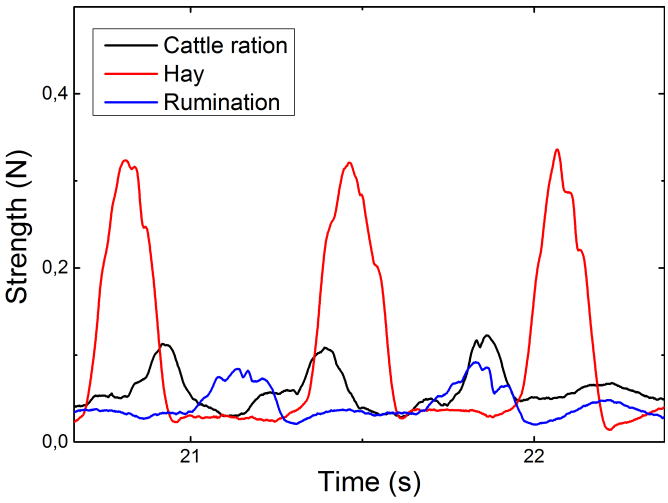

Fig. 14. Graph showing the detected force (N) for some types of chewed food, including rumination, in relation to time (s).

chewing process for ingestion of cattle ration, while a longest time (approximately 8 minutes), demonstrating there are no variations in signal base line, its indicate that the temperature was not change, as expected due to the homeostasis state of the animal.

Fig. 14 depicts detected forces *versus* time during the chewing process for ingestion of some foods provided to the animal, including the rumination process. Signals are superimposed, a relative time gap/stamp was chosen to demonstrate the signal pattern for each food for two or three chewing cycles. The choice was purely random.

The detected force in the sensor is proportional to the mechanical deformation in the sensor attachment region, i.e., the higher the amplitude of the signal, the higher is the mechanical strain on the mandible.

It is possible to observe that the signal amplitude depends on the hardness of the material chewed by the animal. Another factor affecting the signal is the range of movements that the animal needs to perform to complete the chewing motion.

Specifically, in the signal relative to the chewing of the cattle ration, one can notice a more irregular response from the sensor. The cause is probably associated to painful inhibitory reflexes caused by the biting of a harder material. Such reflexes induce an abrupt loss of the masticatory force and a stretch in the periodontal ligament to prevent damage to teeth or surrounding tissues.

By analyzing the force during the hay chewing, there is a significant change in the load detected by the FBG sensor, since the animal needs to perform large range of motion because the food is dehydrated and presents higher concentration of fibers.

From the rumination signal, it is clear that the signal amplitude is small, meaning that low deformation levels occurred. In rumination process, the pre-chewed food returns to the animal's mouth, with more saliva, forming a soft paste that is re-chewed and thus presents lower deformation levels.

Data obtained were processed by the patterns classifier described in [20], which provided an average classification success rate of 94%.

IV. Conclusion

The sensor calibration provided a good strain sensitivity because it was able to detect and discriminate forces lower than 0.1 N. A good linearity was also identified; as the relationship between mechanical deformation and wavelength presented a correlation coefficient of 0.9987. The sensor-combined uncertainty calculation demonstrated an uncertainty of 0.027 N in the results.

It was possible to verify that the developed biosensor is suitable for data acquisition during masticatory movements of a living animal. The acquired signals show good signal-to-noise ratio, thus enabling the interpretation of different masticatory patterns, with different force magnitude and frequency contents, associated to the animal's chewing process.

This biosensor features a few advantages in addition to its high sensitivity, linearity, reduced size, biocompatibility, and immunity to electromagnetic interference. The automated acquisition and data processing stands out. In addition, a minimally invasive procedure is required for its implantation into animals.

From this research, it can be concluded that the developed biosensor can help one to understand bone tissue behavior in very specific situations, such as masticatory movement analysis. Prospectively, it may also be used to analyze other events that affect bone tissues, such as fractures and degenerative processes, and assist in biomechanics study and prostheses development.

References

[1] H. M. Frost, "A 2003 update of bone physiology and Wolff's law for clinicians," *Angle Orthodontist*, vol. 74, no. 1, pp. 3–15, 2004.

[2] R. Huiskes, R. Ruimerman, G. H. van Lenthe, and J. D. Janssen, "Effects of mechanical forces on maintenance and adaptation of form in trabecular bone," *Nature*, vol. 405, pp. 704–706, Jun. 2000.

[3] D. R. Carter, G. S. Beaupré, N. J. Giori, and J. A. Helms, "Mechanobiology of skeletal regeneration," *Clin. Orthopaedics Rel. Res.*, vol. 355, pp. S41–S55, Oct. 1998.

[4] W. M. Clapham, J. M. Fedders, K. Beeman, and J. P. S. Neel, "Acoustic monitoring system to quantify ingestive behavior of free-grazing cattle," *Comput. Electron. Agricult.*, vol. 76, no. 1, pp. 96–104, Mar. 2011.

[5] E. A. Laca, E. D. Ungar, N. G. Seligman, M. R. Ramey, and M. W. Demment, "An integrated methodology for studying short-term grazing behaviour of cattle," *Grass Forage Sci.*, vol. 47, no. 1, pp. 81–90, Mar. 1992.

[6] A. G. Deswysen, P. Dutilleul, J. P. Godfrin, and W. C. Ellis, "Nycterohemeral eating and ruminating patterns in heifers fed grass or corn silage: Analysis by finite Fourier transform," *J. Animal Sci.*, vol. 71, no. 10, pp. 2739–2747, 1993.

[7] P. S. Mir, C. M. Kalnin, and S. A. Garvey, "Recovery of fecal chromium used as a digestibility marker in cattle," *J. Dairy Sci.*, vol. 72, no. 10, pp. 2549–2553, Oct. 1989.

[8] G. M. Van Dyne and H. F. Heady, "Botanical composition of sheep and cattle diets on a mature annual range," *J. Agricult. Sci.*, vol. 36, no. 13, pp. 465–492, 1965.

[9] P. Roriz, L. Carvalho, O. Frazão, J. L. Santos, and J. A. Simões, "From conventional sensors to fibre optic sensors for strain and force measurements in biomechanics applications: A review," *J. Biomech.*, vol. 47, no. 11, pp. 1251–1261, Apr. 2014.

[10] G. Wehrle, P. Nohama, H. J. Kalinowski, P. I. Torres, and L. C. G. Valente, "A fibre optic Bragg grating strain sensor for monitoring ventilatory movements," *Meas. Sci. Technol.*, vol. 12, no. 7, pp. 805–809, 2001.

[11] S. C. Tjin, Y. K. Tan, M. Yow, Y.-Z. Lam, and J. Hao, "Recording compliance of dental splint use in obstructive sleep apnoea patients by force and temperature modelling," *Med. Biol. Eng. Comput.*, vol. 39, no. 2, pp. 182–184, Mar. 2001.

[12] K. O. Hill, Y. Fujii, D. C. Johnson, and B. S. Kawasaki, "Photosensitivity in optical fiber waveguides: Application to reflection filter fabrication," *Appl. Phys. Lett.*, vol. 32, no. 10, pp. 647–649, 1978.

[13] H. J. Kalinowski, I. Abe, J. A. Simões, A. Ramos, "Application of fibre Bragg grating sensors in biomechanics," in *John Canning. (Org.)*, vol. 1, ch. 10, Trivandrum, India: Transworld Research Network, 2010, pp. 315–345.

[14] M. S. Milczewski, J. C. C. Silva, L. M. Carvalho, J. Canning, "Optical fibre sensors in dentistry," in *John Canning. (Org.)*, vol. 1, ch. 11, Trivandrum, India: Transworld Research, 2010, pp. 345–373.

[15] C. R. Dennison *et al.*, "*Ex vivo* measurement of lumbar intervertebral disc pressure using fibre-Bragg gratings," *J. Biomech.*, vol. 41, no. 1, pp. 221–225, 2008.

[16] S. J. Mihailov, "Fiber Bragg grating sensors for harsh environments," *Sensors*, vol. 12, no. 2, pp. 1898–1918, 2012.

[17] L. Carvalho, N. J. Alberto, P. S. Gomes, R. N. Nogueira, J. L. Pinto, and M. H. Fernandes, "In the trail of a new bio-sensor for measuring strain in bone: Osteoblastic biocompatibility," *Biosensors Bioelectron.*, vol. 26, no. 10, pp. 4046–4052, Jun. 2011.

[18] Y.-J. Rao, D. J. Webb, D. A. Jackson, L. Zhang, and I. Bennion, "In-fiber Bragg-grating temperature sensor system for medical applications," *J. Lightw. Technol.*, vol. 15, no. 5, pp. 779–785, May 1997.

[19] C. Wosniak *et al.*, "Determination of chewing patterns in goats using fiber Bragg gratings," in *Proc. SPIE 22nd Int. Conf. Opt. Fiber Sens.,* Beijing, China, vol. 8421, pp. 84214F-1–84214F-4. 2012.

[20] V. Pegorini *et al.*, "*In vivo* pattern classification of ingestive behavior in ruminants using FBG sensors and machine learning," *Sensors*, vol. 15, no. 11, pp. 28456–28471, 2015.

[21] L. Z. Karam *et al.*, "*Ex vivo* determination of chewing patterns using FBG and artificial neural networks," in *Proc. SPIE 23rd Int. Conf. Opt. Fibre Sens.,* Santander, vol. 9157, pp. 91573Z-1–91573Z-4, Jun. 2014.

[22] J. C. C. Silva *et al.*, "Fibre Bragg grating sensing and finite element analysis of the biomechanics of the mandible," *Proc. SPIE 17th Int. Conf. Opt. Fiber Sens.*, Bruges, Belgium, vol. 5855, pp. 102–105, May 2005.

[23] A. Ramos, A. Ballu, M. Mesnard, P. Talaia, and J. A. Simões, "Numerical and experimental models of the mandible," *Experim. Mech.*, vol. 51, no. 7, pp. 1053–1059, Sep. 2011.

[24] M. Niinomi, "Mechanical properties of biomedical titanium alloys," *Mater. Sci. Eng. A*, vol. 243, nos. 1–2, pp. 231–236, Mar. 1998.

[25] D. M. Brunette, P. Tengvall, M. Textor, and P. Thomsen, *Titanium in Medicine*. New York, NY, USA: Springer, 2001, pp. 2–23.

[26] *Avaliação de Dados de Medição: Guia Para a Expressão de Incerteza de Medição—GUM 2008*, 1st ed., Inst. Nacional Metrologia, Qualidade Tecnologia, Rio de Janeiro, Brazil, 2012.

[27] L. Carvalho, J. C. C. Silva, R. N. Nogueira, J. L. Pinto, H. J. Kalinowski, and J. A. Simões, "Application of Bragg grating sensors in dental biomechanics," *J. Strain Anal. Eng. Des.*, vol. 41, no. 6, pp. 411–416, 2006.
[28] L. Z. Karam, A. P. Franco, P. Tomazinho, and H. J. Kalinowski, "Validation of a sterilization methods in FBG sensors for *in vivo* experiments," presented at the LAOP, 2012. [Online]. Available: https://www.osapublishing.org/abstract.cfm?uri=LAOP-2012-LT2A.7
[29] C.-H. Zhang *et al.*, "Use of absorbable hemostatic gauze with medical adhesive is effective for achieving hemostasis in presacral hemorrhage," *Amer. J. Surgery*, vol. 203, no. 4, pp. e5–e8, Apr. 2012.
[30] S. Bugden *et al.*, "Skin glue reduces the failure rate of emergency department–inserted peripheral intravenous catheters: A randomized controlled trial," *Ann. Emerg. Med.*, vol. 68, no. 2, pp. 196–201, Aug. 2016.

Alessandra Kalinowski, photograph and biography not available at the time of publication.

Leandro Zen Karam, photograph and biography not available at the time of publication.

Vinicius Pegorini, photograph and biography not available at the time of publication.

André Biffe Di Renzo, photograph and biography not available at the time of publication.

Christiano Santos Rocha Pitta, photograph and biography not available at the time of publication.

Rafael Cardoso, photograph and biography not available at the time of publication.

Tangriani Simioni Assmann, photograph and biography not available at the time of publication.

Hypolito José Kalinowski, photograph and biography not available at the time of publication.

Jean Carlos Cardozo da Silva, photograph and biography not available at the time of publication.